FATIGUE CRACK GROWTH IN 2024-T3 ALUMINUM UNDER TENSILE AND TRANSVERSE SHEAR STRESSES[1]

113074

Mark J. Viz[2] and Alan T. Zehnder[2]
Department of Theoretical and Applied Mechanics
Cornell University, Ithaca, New York 14853
(607)255-9181, fax: (607)255-2011, email: atz@msc.cornell.edu

SUMMARY

The influence of transverse shear stresses on the fatigue crack growth rate in thin 2024-T3 aluminum alloy sheets is investigated experimentally. The tests are performed on double-edge cracked sheets in cyclic tensile and torsional loading. This loading generates crack tip stress intensity factors in the same ratio as the values computed for a crack lying along a lap joint in a pressurized aircraft fuselage. The relevant fracture mechanics of cracks in thin plates along with the details of the geometrically nonlinear finite element analyses used for the test specimen calibration are developed and discussed. Preliminary fatigue crack growth data correlated using the fully coupled stress intensity factor calibration are presented and compared with fatigue crack growth data from pure ΔK_I fatigue tests.

INTRODUCTION

Recently the problem of a crack near a lap joint (see figure 1) in the pressurized fuselage of an airplane was recognized as a situation in which material near the crack tip is subjected to both tensile and transverse shear (i.e., out-of-plane tearing) stresses. Concern over the effect of tearing stresses on the fatigue crack growth rate prompted researchers at NASA Langley to sponsor a program of analytical, numerical and experimental research at Cornell University aimed at measuring fatigue crack growth rates in such situations and developing the theory and numerical procedures necessary to interpret and to apply the experimental data.

The lap joint problem is illustrated in figure 1. Crack tip tensile stresses arise from the hoop stress in the fuselage skin, while the out-of-plane tearing stresses arise from the pressure difference "pushing out" on the skin. As shown in figure 1, one side of the crack remains riveted to the stringer and to the adjoining skin forming the lap joint. This side of the crack is much stiffer than the other side which is only a single sheet thick. This less stiff side bulges out relative to the stiff side, resulting in tearing stresses at the crack tip.

The stresses at the crack tip resulting from this loading can be described as a combination of membrane stresses constant through the thickness and transverse shear or tearing stresses that have a through the thickness variation. As defined in figure 2, for general loadings of thin, cracked plates under membrane and out-of-plane loads, two fracture modes with corresponding stress intensity factors K_I and K_{II} can be identified with the membrane loads, and two fracture modes with stress intensity factors k_1 and k_2 can be identified with the out-of-plane loads.

[2] Graduate Research Assistant and Assistant Professor, respectively.

Assuming that the crack tip stresses are a superposition of the stresses from the membrane and out-of-plane loads, and that the out-of-plane part can be described using Kirchhoff plate theory, the stresses on a plane ahead of the crack ($\theta = 0$ in the coordinate system of figure 3) are [1-3]

$$\sigma_{22} = \frac{K_I}{\sqrt{2\pi r}} + \frac{k_1}{\sqrt{2r}} \frac{2x_3}{h},$$

$$\sigma_{12} = \frac{K_{II}}{\sqrt{2\pi r}} + \frac{k_2}{\sqrt{2r}} \left(\frac{1+\nu}{3+\nu}\right) \frac{2x_3}{h}, \qquad (1)$$

$$\sigma_{23} = \frac{-k_2 h}{2(2r)^{3/2}(3+\nu)} \left[1 - \left(\frac{2x_3}{h}\right)^2\right],$$

where ν is the Poisson ratio and h is the plate thickness. The in-plane stress components, σ_{12} and σ_{22}, each have a constant and linear thickness variation term resulting from membrane and bending loads. The out-of-plane stress component, σ_{23}, varies parabolically through the thickness of the plate and has an $r^{-3/2}$ singularity, a manifestation of the limitation of Kirchhoff plate theory to satisfy completely the natural boundary conditions occurring at a free crack surface. Note the absence of $1/\sqrt{\pi}$ in the k_1, k_2 terms. This makes the definitions of k_1 and k_2 correspond to those introduced by Sih et al.[3] and is the form adopted by handbooks of stress intensity factors[4]. For more details and references on crack tip fields in plates loaded out-of-plane see [5,6].

Hui and Zehnder[6] argue that crack initiation and growth in thin plates under combined membrane and out-of-plane loads can be correlated with the stress intensity factors K_I, K_{II}, k_1 and k_2 (see eq. (1)). For the lap joint crack it appears that only K_I and k_2 are significant. The other two stress intensity factors are zero or nearly zero in this case. The relative importance of the tension and tearing stresses can be assessed by computing the K_I and k_2 for a crack located along the lap joint and comparing the values. Such a computation was performed by Britt[7] and is summarized here in figure 4 where the geometry of the problem is shown, and the stress intensity factor k_2 is plotted against K_I for a variety of crack lengths. For the crack situated along the stringer k_2 becomes comparable to K_I. A second scenario in which k_2 is relatively large occurs for a curved crack in a fuselage as studied by Potyondy et al.[8]. In this problem, the growth of a curving crack is simulated; high values of k_2 with respect to K_I were found to occur.

In both cases, for longer cracks k_2 becomes significant and thus may be an important factor in determining fatigue crack growth rate. Whether this is true or not is one of the principal subjects of this research. An extensive literature search revealed no data on fatigue fracture under such loadings, thus we are undertaking a series of fatigue crack growth rate experiments such that the K_I and k_2 stress intensity factors are imposed.

NUMERICAL PROCEDURES

To correlate crack growth rate with K_I and k_2, the capability to compute these stress intensity factors for both the test specimen and for the aircraft fuselage structure is needed. Numerical analyses are necessary for this computation since the stress intensity factor handbooks do not contain k_2 solutions for finite dimensional plates that would be used for experimentation. The procedure used here is to compute components of the energy release rate from finite element analyses and then calculate K_I and k_2 from the relations between stress intensity factors and these components of the energy release rate.

The energy released during crack growth is equal to the work done by the tractions acting over the area of crack extension. For a linearly elastic plate of thickness h the energy release rate, G, for self-similar extension of a through crack lying in the x_1, x_3 plane is[9,10]

$$G = \lim_{\Delta L \to 0} \frac{1}{2h\Delta L} \int_0^{\Delta L} \int_{-h/2}^{+h/2} \sigma_{2i}(x_1, \theta = 0)\Delta u_i(\Delta L - x_1, \theta = \pi)dx_3 dx_1, \qquad (2)$$

where Δu_i are the components of relative crack tip displacement for a crack extension of ΔL, and the repeated index i implies summation over $i = 1, 2, 3$.

From this statement of the energy release rate the relationship between G and the stress intensity factors can be found[6]. The stress and displacement fields from Williams[1,2] are substituted into eq. 2, and after some manipulation and grouping of the membrane terms and the bending terms, the following relationships between the G components and the stress intensity factors are found

$$\begin{aligned}
G_1 &= \frac{K_I^2}{E}, \\
G_2 &= \frac{K_{II}^2}{E}, \\
G_4 &= \frac{k_1^2 \pi}{3E}\left(\frac{1+\nu}{3+\nu}\right), \\
G_3 + G_5 &= \frac{k_2^2 \pi}{3E}\left(\frac{1+\nu}{3+\nu}\right).
\end{aligned} \qquad (3)$$

For a general loading the total energy release rate is the sum of the above, i.e.,

$$G = G_1 + G_2 + G_3 + G_4 + G_5. \qquad (4)$$

The numbering of the components of G is arbitrary; the numbering convention chosen corresponds to the numbering of the degrees of freedom in the finite element program used for the stress intensity factor calculations. If the separate terms of the energy release rate in eq. 3 can be found from a numerical analysis, then eq. 3 can be used to calculate all four stress intensity factors.

To validate the method for the calculation of K_I, K_{II}, k_1 and k_2, six test analyses of finite cracks in infinite plates were conducted. Figure 5 shows these sample problems along with their theoretical solutions taken from refs. 3 and 6. Three of these test cases involve only a single mode; thus, the virtual crack extension technique [11-14] is appropriate to compute the single stress intensity factor in each of these problems. This technique gives only a total G value as its result; consequently, it must be known *a priori* what single mode is present. The other three test cases involve loadings which generate mixed modes at the crack tip. For these cases, the nodal release method [15] is necessary to be able to compute the individual G_is and hence the relevant stress intensity factors. The nodal release method computes the components of G on a nodal degree of freedom basis such that each G_i component is related to one of the four fracture modes shown in figure 2.

The computations of figure 5 as well as the test specimen calibrations discussed later were performed using the STAGS (STructural Analysis of General Shells) code[16]. The plate model

had dimensions of 11.0 by 10.0 by 0.090 thick and contained a centrally located straight crack of length 1.0 oriented parallel to the 11.0 dimension. No special crack tip elements were used. Instead, the STAGS 410 element[17], a four-noded, six degree-of-freedom per node flat plate element, was used for the entire mesh. All elements were square inside a near tip region of mesh refinement that extends a distance $\frac{L}{2}$ above and below the crack line and $\frac{L}{4}$ behind and $\frac{L}{2}$ ahead of the crack tip (L is the crack length). The standard element size in this region was $\frac{L}{64}$.

The results of these sample computations are also given in figure 5. For the three single mode cases the virtual crack extension results were all within 3.6% difference from the theoretical solutions. For the three mixed mode cases the nodal release results were all within 1.3% difference from the theoretical solutions. Based on these results the applicability of these two methods for the calculation of the four stress intensity factors is established.

However, for the stress intensity factor calculations needed for the calibration of the test specimen both the virtual crack extension technique and the nodal release technique have significant drawbacks. The virtual crack extension technique by its nature does not permit the computation of the individual components of the energy release rate, rendering it useless for a mixed mode situation such as our testing configuration. The nodal release method, although applicable to any general mixed mode situation, has the disadvantage of requiring two full finite element analyses to be performed per one G_i computation. This would double the already large number of required analyses. Consequently, a third method, the modified crack closure integral method[18,19], was used. This method approximates the displacement field over a crack advance of ΔL by using the displacement field behind the crack of length L, thus requiring only a single analysis per stress intensity factor calculation. The results already given that relate components of the energy release rate on a nodal degree of freedom basis to the four stress intensity factors can be applied to the modified crack closure integral method.

EXPERIMENTAL METHOD

To determine the fatigue crack growth rate as a function of the two stress intensity factors K_I and k_2, double-edge cracked plates were tested under constant amplitude cyclic tensile and torsional loadings. The test specimens were machined from 2.29mm thick 2024-T3 aluminum plates provided by NASA Langley. This is the same batch of aluminum sheets used by Hudson[20] in his pure mode I fatigue crack growth study in 1969. The test specimen dimensions and geometry are shown in figure 6. On each side of the test specimen a 6.35mm long, 0.18mm wide starter notch was cut using a foil electric discharge machine. The samples were diamond polished to a 3μm finish to improve the optical crack length measurement.

Ideally, the sample loaded into the gripping fixtures is subjected to uniform vertical displacements (in the y direction; see figure 6) and to a rigid rotation about the y axis at the bottom boundary. Any deviation from this condition will change the stress distribution, and consequently the stress intensity factors and rate of crack growth. To prevent any slipping of the test specimen during a fatigue test, the gripping fixtures and face plates each had two channels cut along their wide direction, into which were inserted 1.52mm diameter steel rods, as shown in figure 6. Sandwiching the specimen between fixtures and face plates and tightening the bolts pushes the steel rods into the specimen creating a slight indentation which then ensures a maintainable grip line for the duration of the fatigue test.

All of the tests were performed using an Instron 1321 tension-torsion servohydraulic test frame operating in tension and torque control. The sample, fixtures and part of the testing machine are shown in figure 7. The testing conditions were monitored continuously with an oscilloscope as well as with a computer that digitized the load, stroke, torque and rotation signals. A 2.54mm long fatigue precrack was grown from each starter notch by cycling with a pure tension load at 6Hz with $\Delta K_I \approx 5.5 MPa\sqrt{m}$ and $R = 0.7$, where $R \equiv P_{min}/P_{max}$, P being the axial tensile load. Typically 100,000 cycles were required for the fatigue precracking.

Testing was performed at $R = 0.7$ for both the tensile and torsional loads. The tensile loads ranged from approximately 2kN to 45kN, and the torques ranged from approximately 11Nm to 110Nm. A thin plate has a relatively low torsional stiffness, thus the specimen experiences large rotations (on the order of 20° for a torque of 110Nm) severely limiting the testing frequency compared to a pure tension loading test. Above 1Hz the testing machine actuator could not maintain the command signal, thus all of the tests were performed at 1Hz where the loads could be controlled to better than 1.0%.

Crack lengths were measured approximately every 0.5mm of crack growth and were recorded with the corresponding number of elapsed cycles as well as the loading conditions. These crack lengths were measured using two travelling microscopes, one for each crack, mounted to the testing frame. Vertical and horizontal microscope movements were measured with digital travel indicators to give an (x, y) location of the crack tip at each measurement. When setting up the test the microscopes were rotated to be normal to the plane of the center of the specimen when the mean torque was applied. This initial rotation was maintained throughout the test. Fluorescent light reflected onto the specimen surface with a sheet of white card stock was used to illuminate the crack tip region. With this arrangement crack length could be measured to an accuracy of ± 0.05mm.

TEST SPECIMEN CALIBRATION

A calibration is needed to relate experimentally measurable quantities, such as the applied loads and crack length, to the stress intensity factors. For the current experiments, P, the net tension load, T, the net torque and, a, the crack length are inputs to a calibration function with the stress intensity factors, K_I and k_2, as output. What makes the calibration for this testing arrangement difficult is that K_I is not solely a function of P and a and k_2 is not solely a function of T and a; on the contrary, K_I and k_2 are both nonlinear functions of P, T and a. Perhaps a simpler way of stating this disregarding the fracture mechanics is that the axial stiffness as well as the torsional stiffness of the specimen are not just functions of the plate geometry but functions of the plate geometry and the current loading of the plate. To approach this aspect of the experimental work it was deemed early on that a numerical approach would be needed to compute the correct stress intensity factor calibration. The approach thus employed is a fully geometrically nonlinear plate finite element analysis.

The means used to calculate the stress intensity factors from the results of a finite element computation were described in a previous section. Using a half-plate model (see figure 6 for modelling details and boundary conditions) and the modified crack closure integral method to obtain the G_i values, geometrically nonlinear analyses were performed for a grid of P, T values at five discrete crack lengths: 6.35mm, 12.7mm, 19.05mm, 25.4mm and 31.75mm, chosen to span the

experimental results which are for crack lengths from 6.0mm to approximately 32.0mm. The K_I calibration "surface" as a function of P, T for three crack lengths (6.35mm, 19.05mm, 31.75mm) is given in figure 8. The corresponding k_2 calibration for the same crack lengths is given in figure 9.

Although these calibration plots exhibit many interesting features only a few will be discussed here. Notice that for higher torque values K_I becomes less sensitive to increasing axial load (see figure 8). This is especially conspicuous for the shortest crack length. Also notice that k_2 at higher torque levels decreases as the axial load is increased (see figure 9). This effect is a result of the dependence of the torsional stiffness on the axial tension load in that as the axial load is increased, the torsional stiffness of the plate also increases.

Further results from the calibration calculations although not shown in figures 8 and 9 also show that K_{II} and k_1 are small compared to K_I and k_2, respectively, though they are present[7,8]. This result is a welcome one, since the crux of this research depends on the near tip stress field in the test specimen being essentially the same as the near tip field in the actual cracked aircraft fuselage. Simulations of crack growth in fuselage bays show that indeed the K_{II} and k_1 components are small compared to K_I and k_2, respectively.

MIXED MODE FATIGUE CRACK GROWTH RATE DATA

The experiments completed to date cover a wide range of cyclic loadings. The stress intensity factors corresponding to these tests were calculated based on the calibration curves of figures 8 and 9 and the maximum values at the start of a test and the end are plotted as the dashed lines in figure 4. This figure shows that the experiments cover the lower end of the K_I and k_2 range for a crack lying along a stringer in a lap joint.

Results from two of the tests are presented here. Analysis of the remaining twenty tests completed to date is in progress. Figures 10 and 11 show the envelopes of stress intensity factors for test nos. 14 and 18. In both tests the torque range was the same, but the axial load in test no. 14 was ten times larger than the axial load range used for test no. 18. In both tests K_I is larger than k_2 for most of the test except for the longest crack lengths in test no. 18.

Fatigue crack growth rates as well as crack length versus elapsed cycles data for each test are shown in figure 12. Shown on the growth plots are benchmark data from Hudson and Newman for pure mode I fatigue crack growth[20,21].

In each test the crack grew intially at a rate close to the pure mode I rate but slowed down dramatically as the crack grew. Thus the $\frac{da}{dN}$ data fell well below the reference lines for longer crack lengths. This appears to be caused by roughness induced crack closure. During an experiment it is observed (by eye and ear) that the crack faces are in contact as they slide with respect to each other. A scanning electron microscope image of the fracture surface (figure 13) shows the region where crack contact has occurred. In this figure the horizontal direction is parallel to the plate surface; the direction of relative crack face sliding is vertical. The fracture surface is flattened out and scoring in the sliding direction is clearly seen.

However, crack growth rate acceleration does occur towards the end of the test data presented in figure 12. It is thought that the crack surface abrasion just mentioned might wear away

enough of the contacting surface that at some critical point this effect is minimized and the crack growth rate once again increases. If this sort of three-phase behavior (i.e., initial pure mode I type growth, then growth rate decrease followed by an increase) is common to all such loading situations for the testing configuration is still unknown, but should be elucidated after all of the test data is analyzed.

DISCUSSION

The experimental data indicate that in the regime of stress intensity factors for which tests were performed the crack growth rate is initially reduced by the presence of k_2 resulting from crack face contact, but that generally this condition does not persist and crack growth rate does eventually increase. Whether this is true at higher values of K_I and k_2 is unclear at this time. Intuitively it would seem logical that by increasing the value of the stresses at the crack tip the crack would grow faster. This may be the case at the higher levels of K_I and k_2 where the crack faces should separate more and crack face contact should not retard crack growth rate. Thus future experiments may concentrate on higher stress intensity factor levels.

SUMMARY AND CONCLUSIONS

Although it is still unclear as to what systematic role, if any, the presence of a k_2 crack tip fracture mode might have on the overall fatigue crack growth rate of a crack in a stiffened fuselage structure, it is clear that characterizing the problem as one of simple mode I fatigue crack growth resulting from the fuselage hoop stress would greatly underestimate the K_I field at the crack tip. Geometrically nonlinear analyses and resultant stress intensity factor calibrations are necessary to describe properly the crack tip stress field in a cracked fuselage lap joint as well as any test specimen configuration used to examine the fatigue crack growth behavior in such structures. Whether or not the presence of the k_2 mode partially drives the fatigue crack growth or if it is simply the additional K_I supplied by the tearing or bulging aspect of the crack through the geometrically nonlinear effects that drives the crack growth is still not resolved.

However, this investigation has seemingly raised as many questions as it may have answered. The question of how to account for crack face contact effectively and what impact it may have on the local loading or unloading of the crack tip is unresolved. Furthermore, the more basic question of whether or not the same phenomenon occurs when a long crack in a fuselage lap joint is flapping is of primary concern as to the relevance of this work to the actual cracked fuselage problem. To complete some fatigue tests at stress intensity factor levels equal to those experienced by an actual cracked fuselage might be required to answer this question definitively. Finally, a quicker and more accurate method of computing all stress intensity factors from a finite element analysis is required.

REFERENCES

[1] Williams, M.L.: On the Stress Distribution at the Base of a Stationary Crack. *Journal of Applied Mechanics*, vol. 24, 1957, pp. 109-114.

[2] Williams, M.L.: The Bending Stress Distribution at the Base of a Stationary Crack. *Journal of Applied Mechanics*, vol. 28, 1961, pp. 78-82.

[3] Sih, G.C.; Paris, P.C.; and Erdogan, F.: Crack Tip Stress- Intensity Factors for Plane Extension and Plate Bending Problems. *Journal of Applied Mechanics*, vol. 29, 1962, pp. 306-312.

[4] Murakami, Y., ed.: *Stress Intensity Factors Handbook – Vol. 2*. Pergammon Press, 1987.

[5] Sih, G.C., ed.: *Mechanics of Fracture 3, Plates and Shells with Cracks*. Noordhoff Int. Pub. Co., 1977.

[6] Hui, C.Y.; and Zehnder, A.T.: A Theory for the Fracture of Thin Plates Subjected to Bending and Twisting Moments. *International Journal of Fracture*, vol. 61, 1993, pp. 211-229.

[7] Britt, V.O.: personal communication. NASA Langley Research Center, Sept. 1993.

[8] Potyondy, D.O.; Wawrzynek, P.A.; and Ingraffea, A.R.: Discrete Crack Growth Analysis Methodology for Through Cracks in Pressurized Aircraft Structures. *Advanced Structural Integrity Methods for Airframe Durability and Damage Tolerance*, NASA CP-3274, 1994.

[9] Irwin, G.R.: Analysis of Stresses and Strains Near the End of a Crack Traversing a Plate. *Journal of Applied Mechanics*, vol. 24, 1957, pp. 361-364.

[10] Rice, J.R.: Mathematical Analysis in the Mechanics of Fracture. *Fracture*, vol. 2, Academic Press, 1968.

[11] Parks, D.M.: A Stiffness Derivative Finite Element Technique for Determination of Elastic Crack Tip Stress Intensity Factors. *International Journal of Fracture*, vol. 10, 1974, pp. 487-502.

[12] Hellen, T.K.: On the Method of Virtual Crack Extensions. *International Journal of Numerical Methods in Engineering*, vol. 9, 1975, pp. 187-207.

[13] deLorenzi, H.G.: Energy Release Rate Calculations by the Finite Element Method. *Engineering Fracture Mechanics*, vol. 21, 1985, pp. 129-143.

[14] Hellen, T.K.; and Blackburn, W.S.: Nonlinear Fracture Mechanics and Finite Elements. *Engineering Computation*, vol. 4, 1987, pp. 2-14.

[15] Ansell, H.: Bulging of Cracked Pressurized Aircraft Structure. *Ph.D. Thesis No. 138*, Institute of Technology, Linkoping, Sweden, Report No. LIU-TEK-LIC-1988:11, 1988.

[16] Almroth, B.O.; Brogan, F.A.; and Stanley, G.M.: Structural Analysis of General Shells. *User Instructions for STAGSC-1*, vol. 2, Lockheed Missiles and Space Co., Report No. LMSC D633873, 1986.

[17] Rankin, C.C.; and Brogan, F.A.: The Computational Structural Mechanics Testbed Structural Element Processor ES5: STAGS Shell Element. *NASA CR4358*, 1991.

[18] Rybicki, E.F.; and Kanninen, M.F.: A Finite Element Calculation of Stress Intensity Factors by a Modified Crack Closure Integral. *Engineering Fracture Mechanics*, vol. 9, 1977, pp. 931-938.

[19] Viswanath, S.; Lakshminarayana, H.V.; and Ravindranath, D.D.: A Modified Crack Closure Integral Method for Calculating Stress Intensity Factors for Cracked Plates Subject to Bending Loads. *International Journal of Fracture*, vol. 41, 1989, pp. R45-R50.

[20] Hudson, C.M.: Effect of Stress Ratio on Fatigue-Crack Growth in 7075-T6 and 2024-T3 Aluminum Alloy Specimens. *NASA TN D5390*, 1969.

[21] Newman, J.C.: personal communication. NASA Langley Research Center, Sept. 1993.
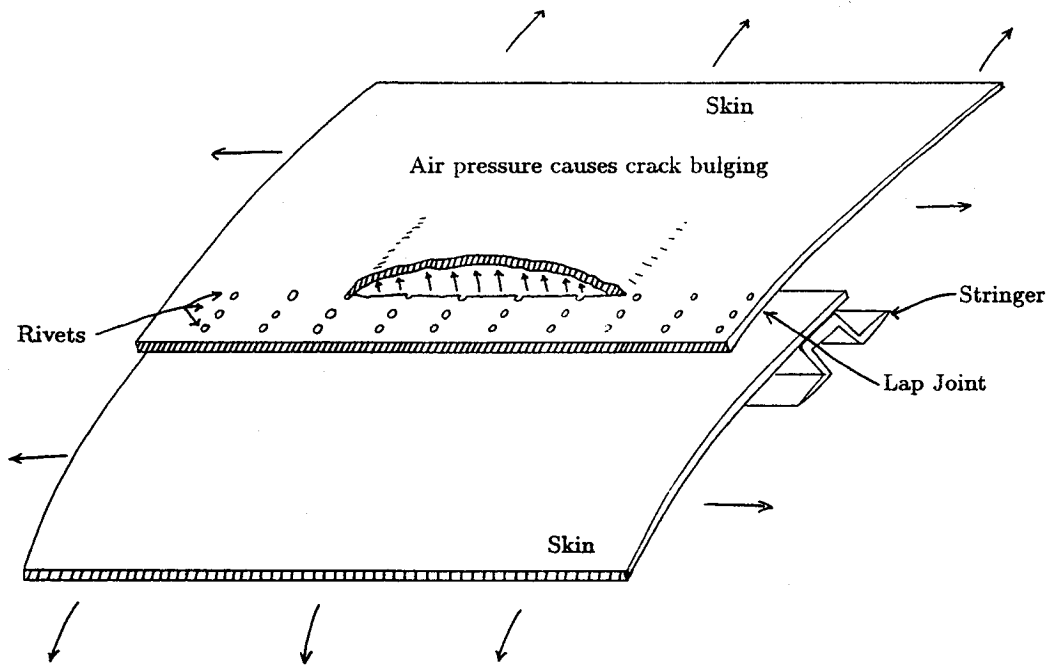
Figure 1. Crack in an aircraft fuselage lap joint along a stringer causing crack face bulging.

Symmetric membrane loading, K_I

Anti-symmetric membrane loading, K_{II}

Symmetric bending, k_1

Anti-symmetric bending and transverse shear, k_2
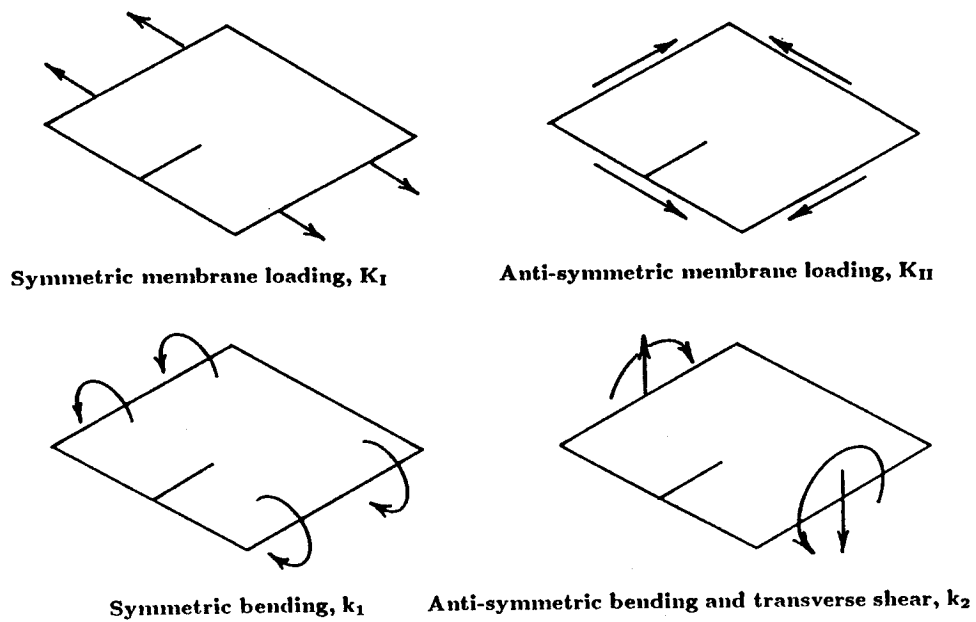
Figure 2. Fracture modes for a thin, cracked plate: K_I, K_{II}, k_1, k_2.

Figure 3. Crack tip coordinate system (see eq. 1).
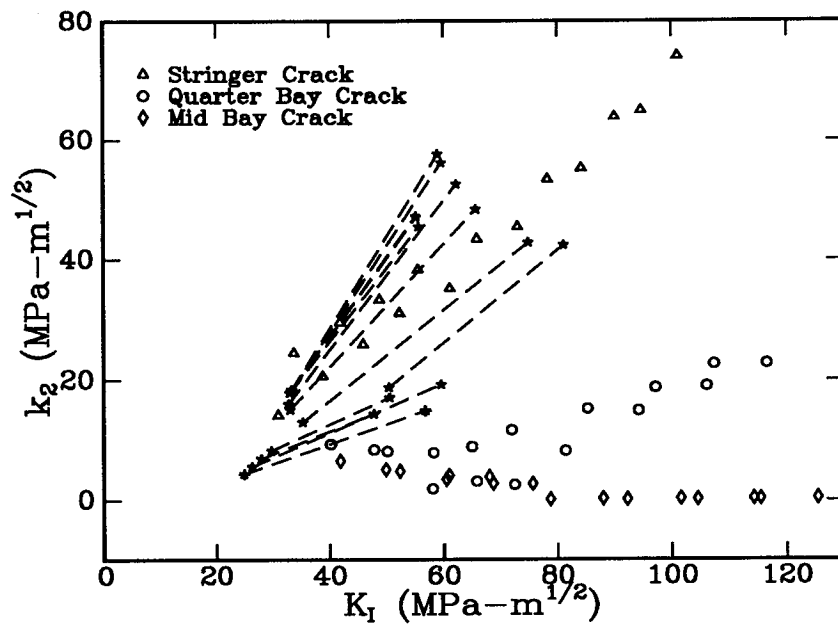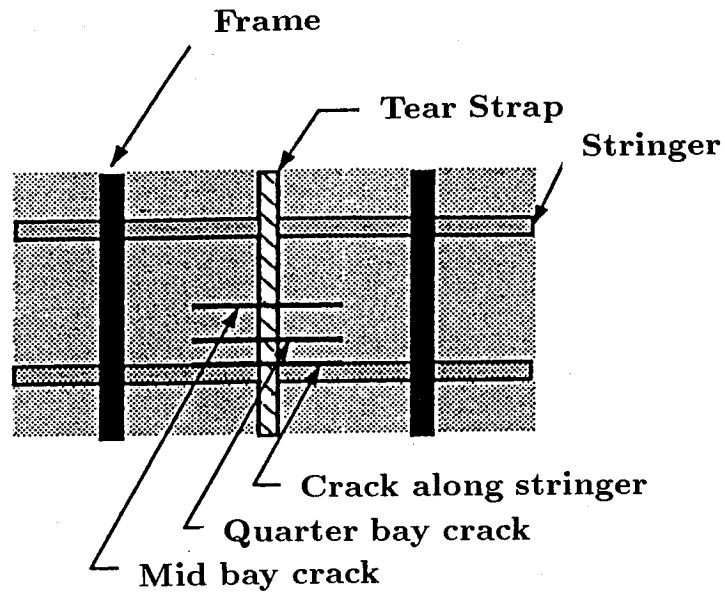
Figure 4. Stress intensity factors, K_I and k_2, for cracks at three positions in a fuselage bay. Points are the computed data from Britt[7]. Dashed lines are the maximum stress intensity factors from the tension-torsion fatigue tests described herein.

Tension

$$K_I = \frac{N_0}{h}\sqrt{\pi a}$$

Tension, Shear, Bending

$$K_I = \frac{N_0}{h}\sqrt{\pi a} \qquad k_1 = \frac{6M_0}{h^2}\sqrt{a}$$

$$K_{II} = \frac{N_{12}}{h}\sqrt{\pi a} \qquad k_2 = 0$$

Bending

$$k_1 = \frac{6M_0}{h^2}\sqrt{a}$$

Bending, Transverse Shear

$$K_I = 0 \qquad k_1 = \frac{6M_0}{h^2}\sqrt{a}$$

$$K_{II} = 0 \qquad k_2 = \frac{3Q_0}{h^2}a^{3/2}$$

Transverse Shear

$$k_2 = \frac{3Q_0}{h^2}a^{3/2}$$

Tension, Transverse Shear

$$K_I = \frac{N_0}{h}\sqrt{\pi a} \qquad k_1 = 0$$

$$K_{II} = 0 \qquad k_2 = \frac{3Q_0}{h^2}a^{3/2}$$
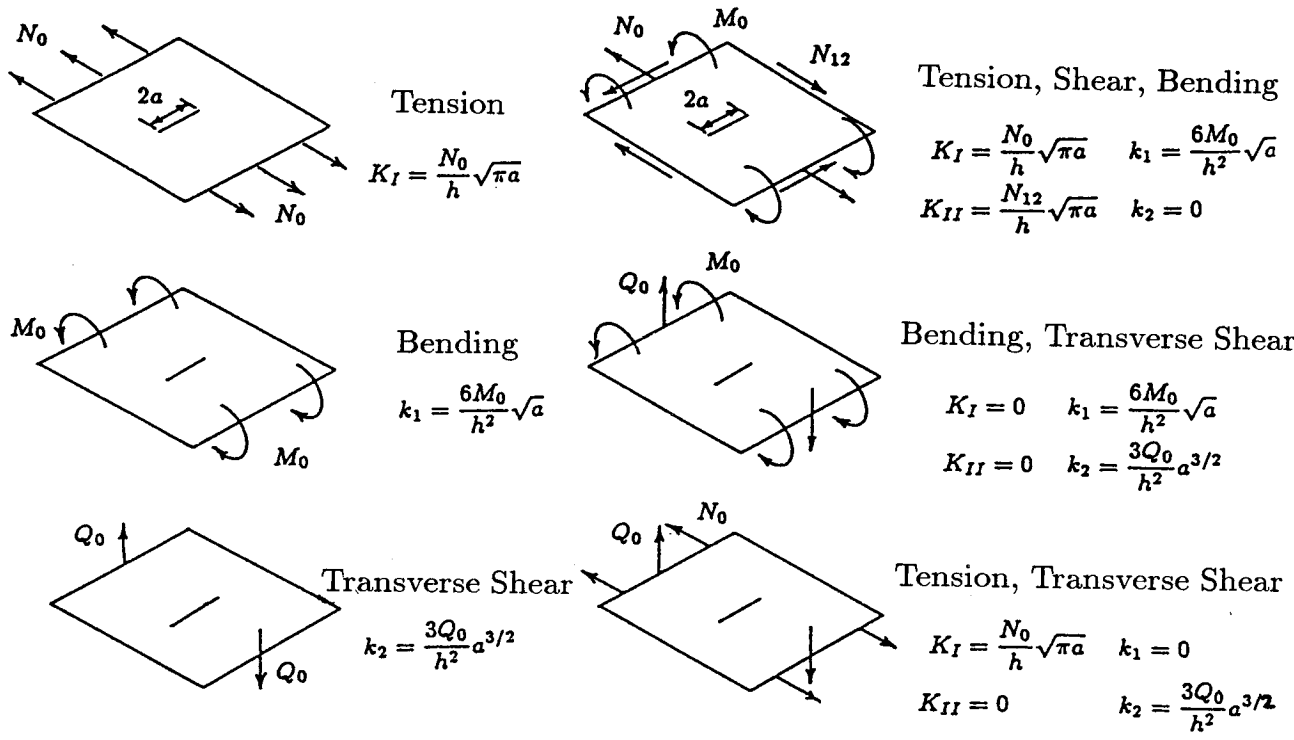
Norm. Theoretical Values	k_1 (6.0)	k_2 (3.0)	K_I (1.7725)	K_{II} (1.7725)
Loading:				
Tension (VCE)[1]	-	-	1.754 (1.0%)	-
Bending (VCE)	5.954 (0.8%)	-	-	-
Transverse Shear (VCE)	-	2.891 (3.6%)	-	-
Tension, Shear & Bending (NR)[2]	5.965 (0.6%)	-	1.765 (0.4%)	1.763 (0.5%)
Bending & Transverse Shear (NR)	5.997 (0.1%)	2.967 (1.1%)	-	-
Tension & Transverse Shear (NR)	-	2.963 (1.3%)	1.760 (0.7%)	-

[1]VCE...virtual crack extension technique
[2]NR...nodal release technique

Figure 5. Six test cases for the validation of the stress intensity factor computation techniques: finite length crack in an infinite plate.
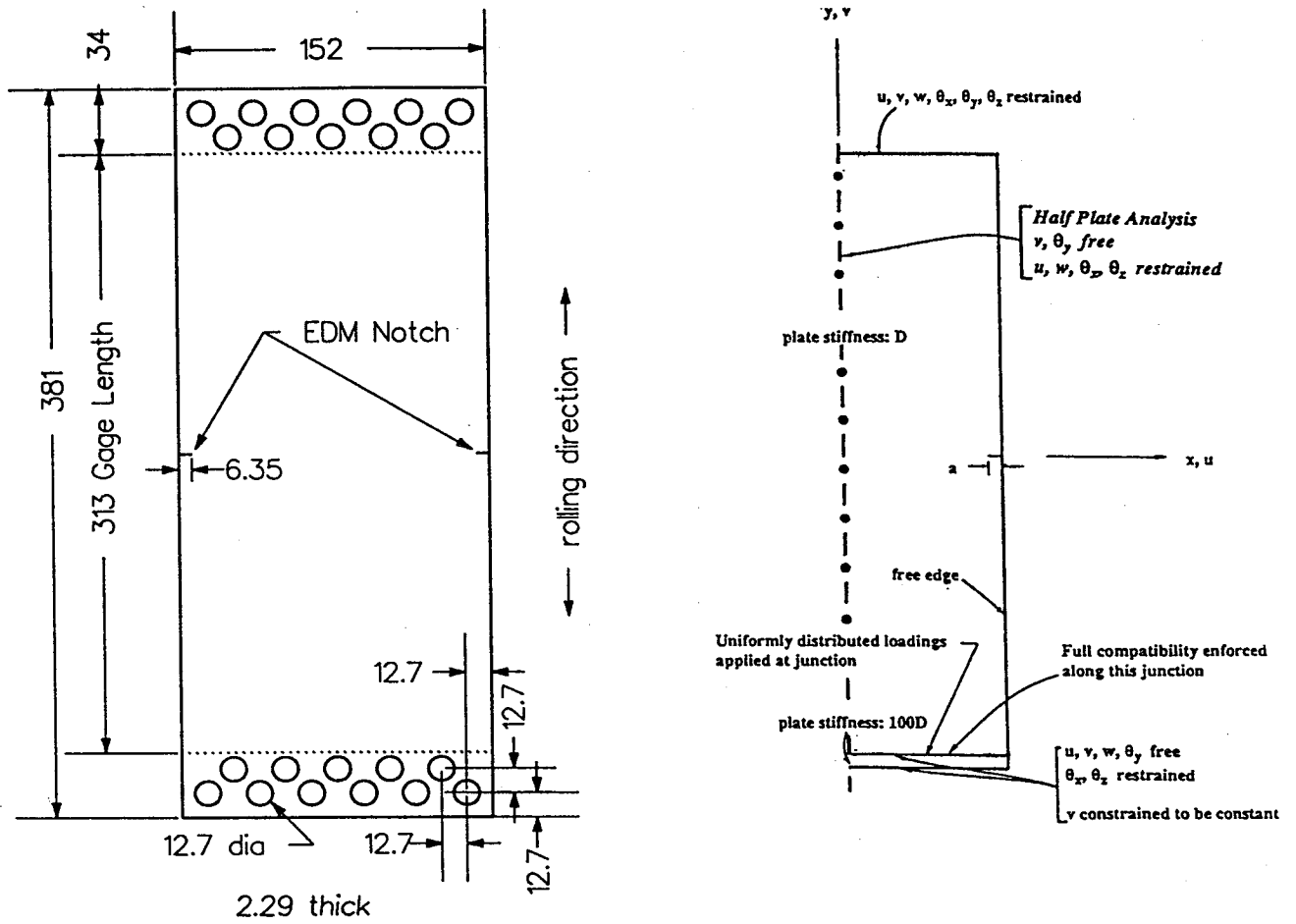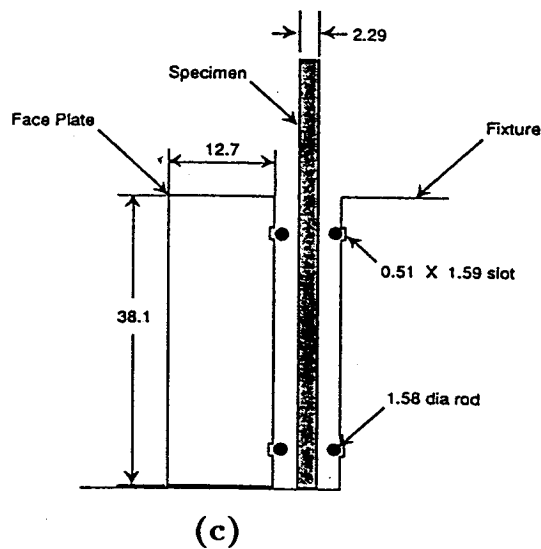
Figure 6. (a) Test specimen, dimensions in mm. (b) Boundary conditions used in finite element model. (c) Detail of specimen gripping fixture.
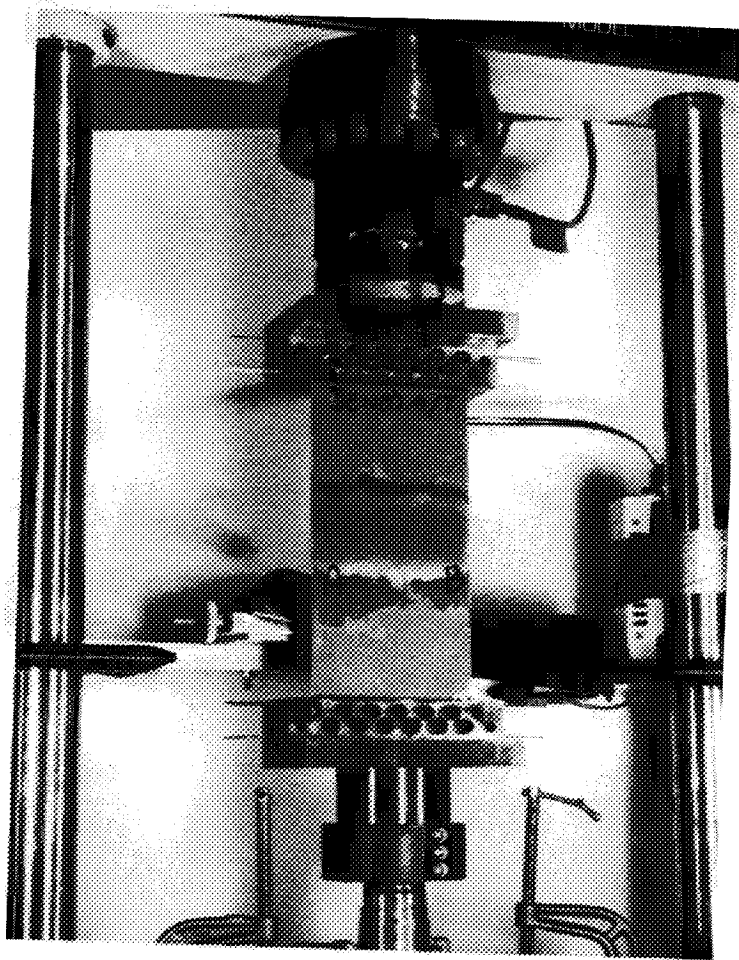
Figure 7. Photograph of the test specimen mounted in the tension-torsion loading frame.
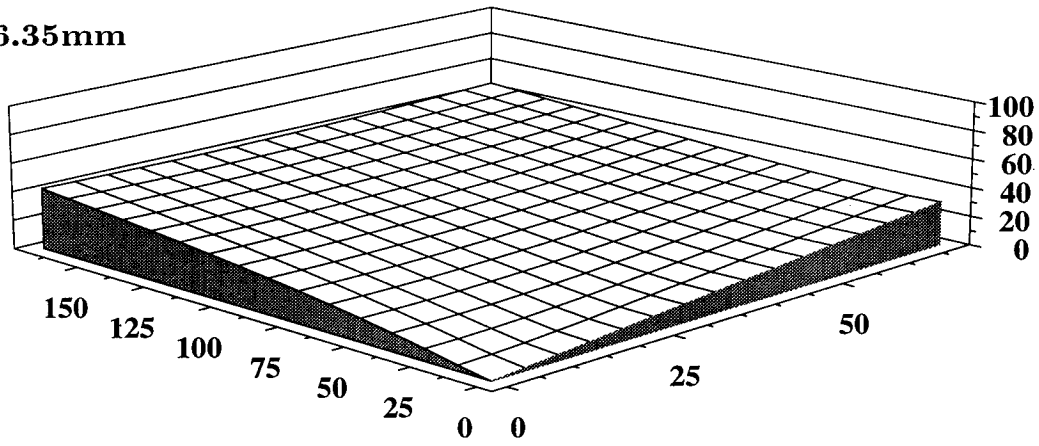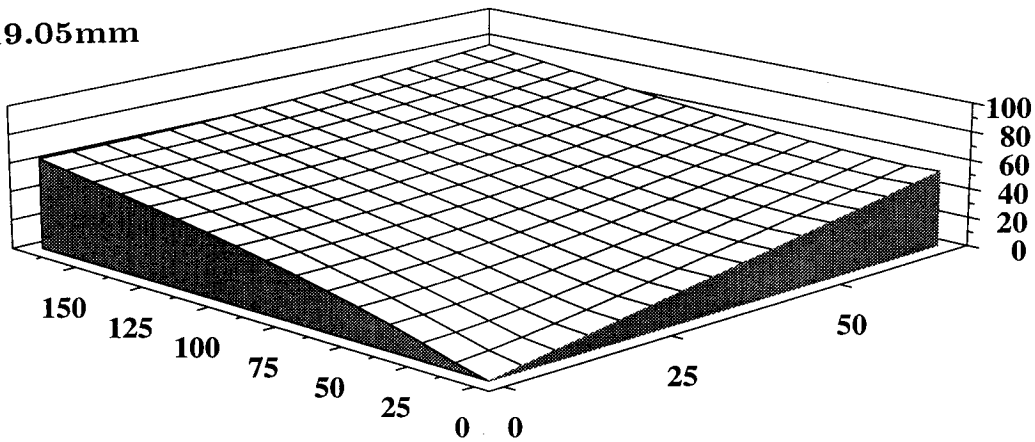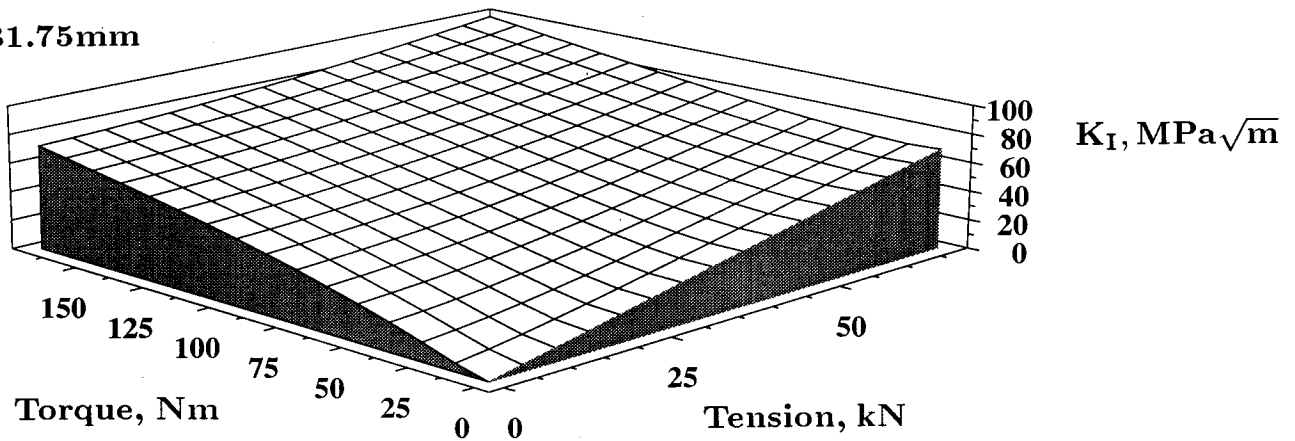
Figure 8. Stress intensity factor K_I versus axial load P and torque T for three crack lengths: 6.35mm, 19.05mm, 31.75mm.
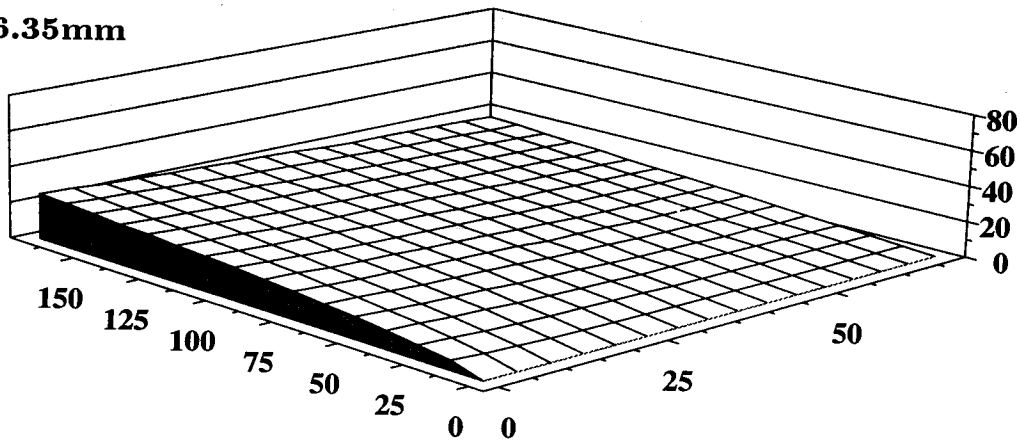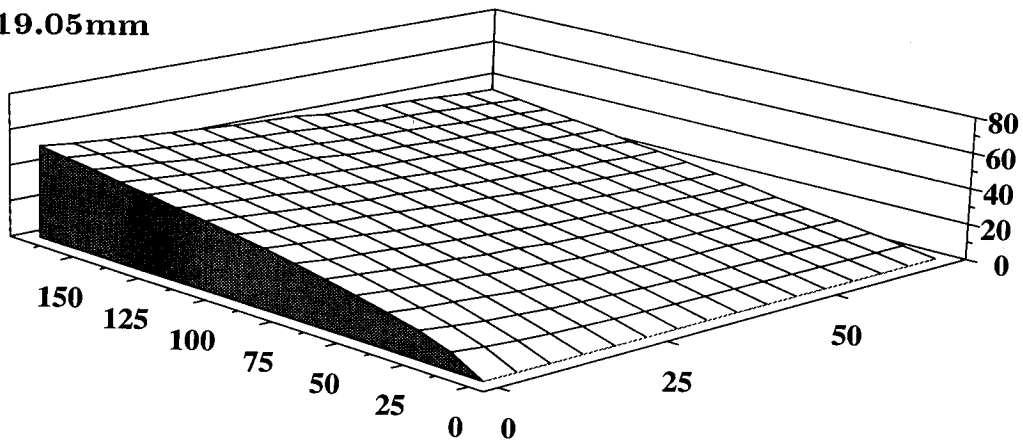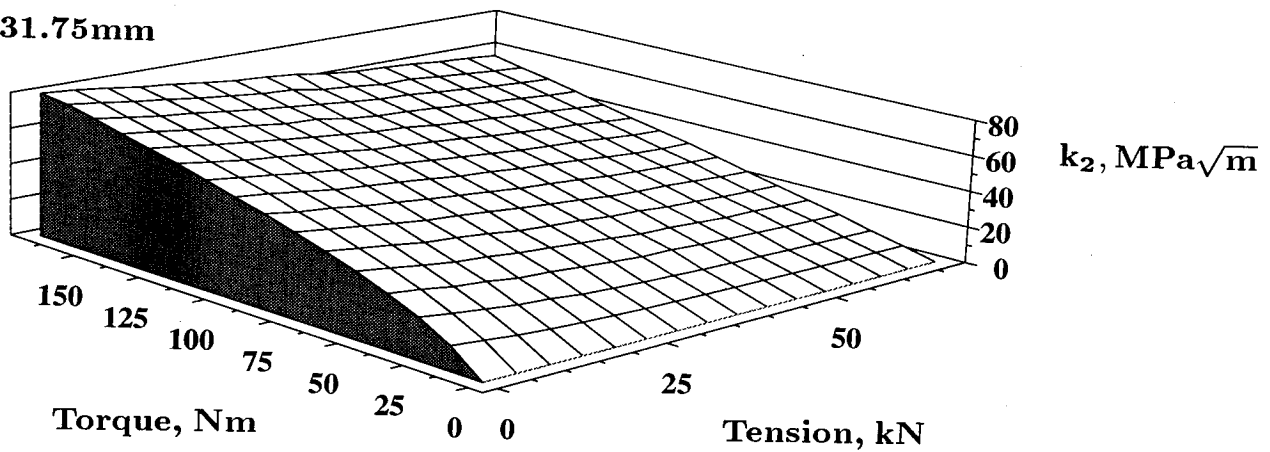
**Figure 9.** Stress intensity factor k_2 versus axial load P and torque T for three crack lengths: 6.35mm, 19.05mm, 31.75mm.
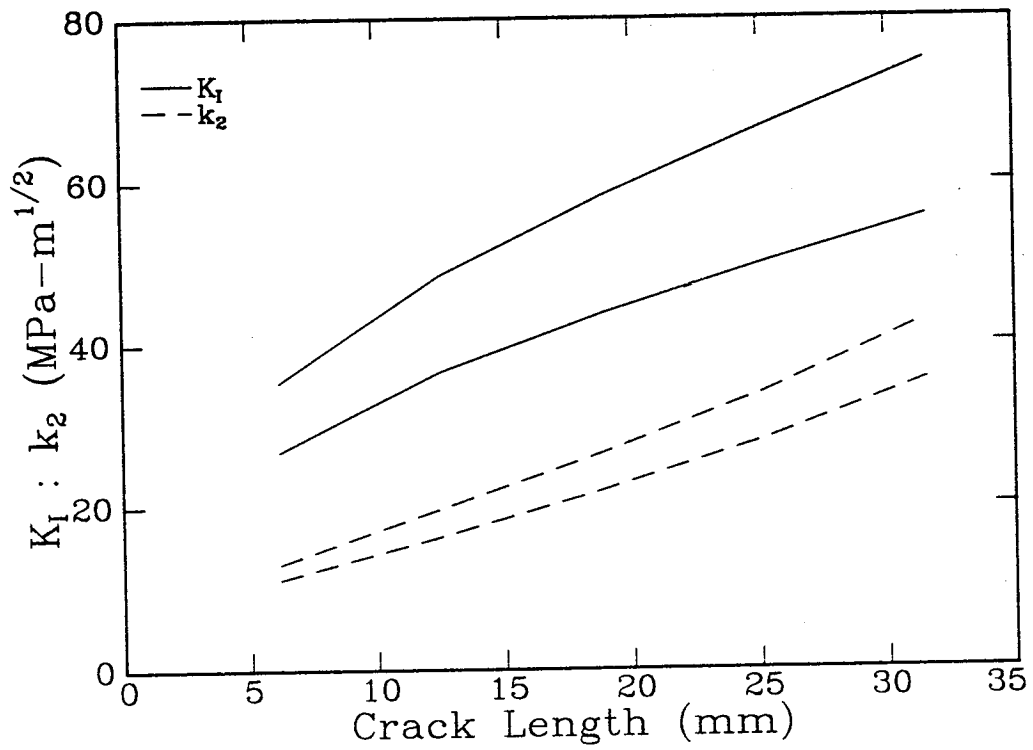
Figure 10. Envelopes of K_I and k_2 versus crack length for test no. 14. (P_{max} =44.5kN, P_{min} =31.2kN, T_{max} =112.0Nm, T_{min} =78.4Nm).
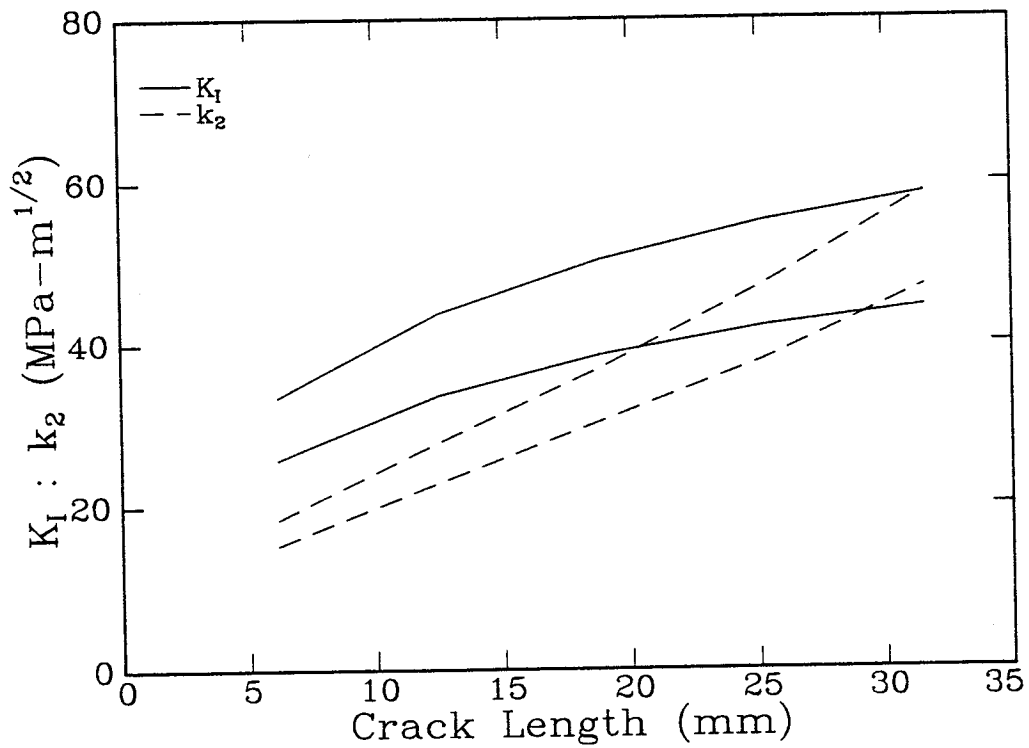
Figure 11. Envelopes of K_I and k_2 versus crack length for test no. 18. (P_{max} =4.5kN, P_{min} =3.1kN, T_{max} =112.0Nm, T_{min} =78.4Nm).
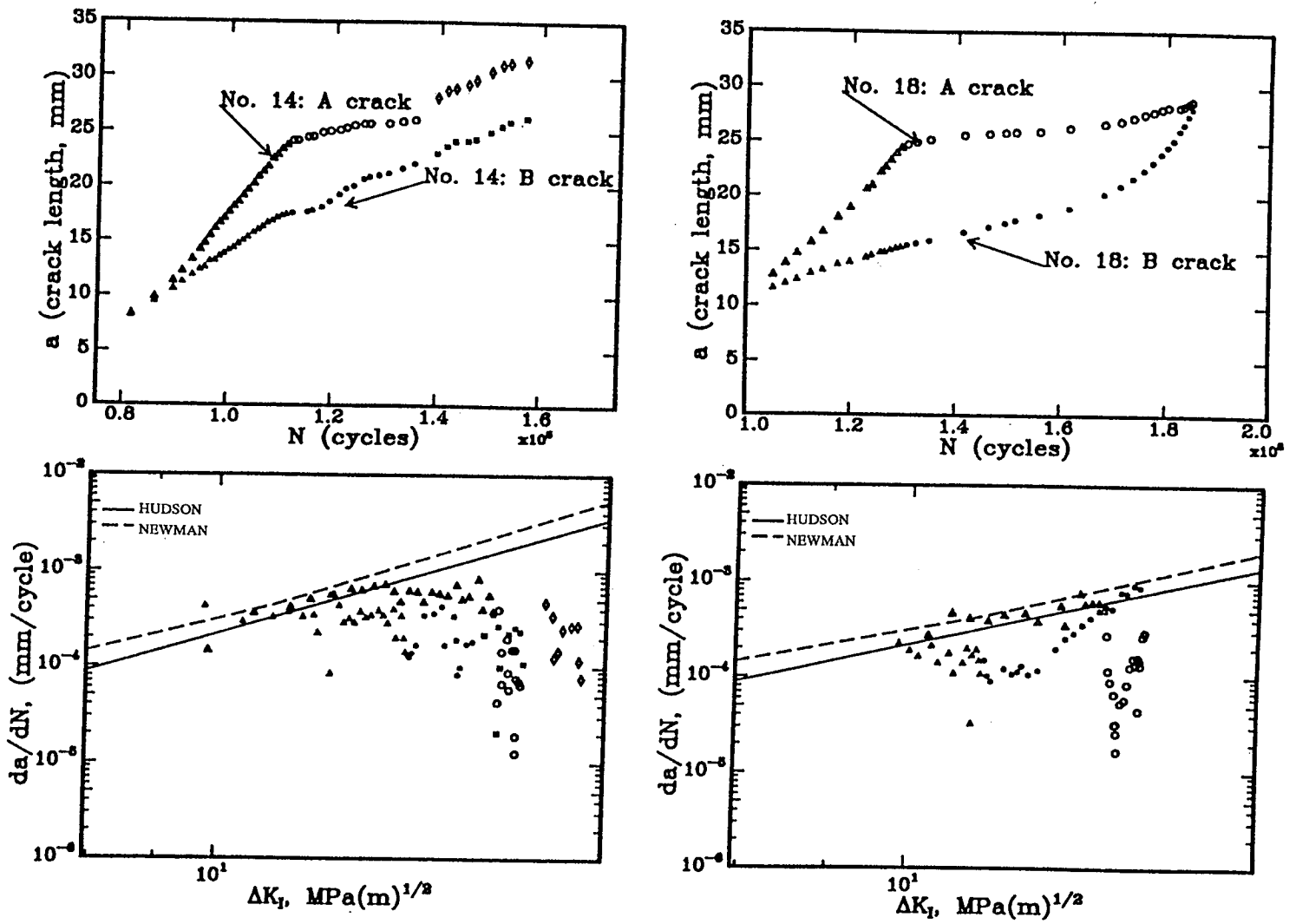
Figure 12. Crack length, a, versus total elapsed cycles, N, and crack growth rate, $\frac{da}{dN}$, versus ΔK_I for test no. 14 (*left*) and test no. 18 (*right*). "A" and "B" designations refer to each of the two cracks in a given specimen. Hudson's[20] pure mode I data is shown by the solid line; Newman's[21] pure mode I data is shown by the dashed line.
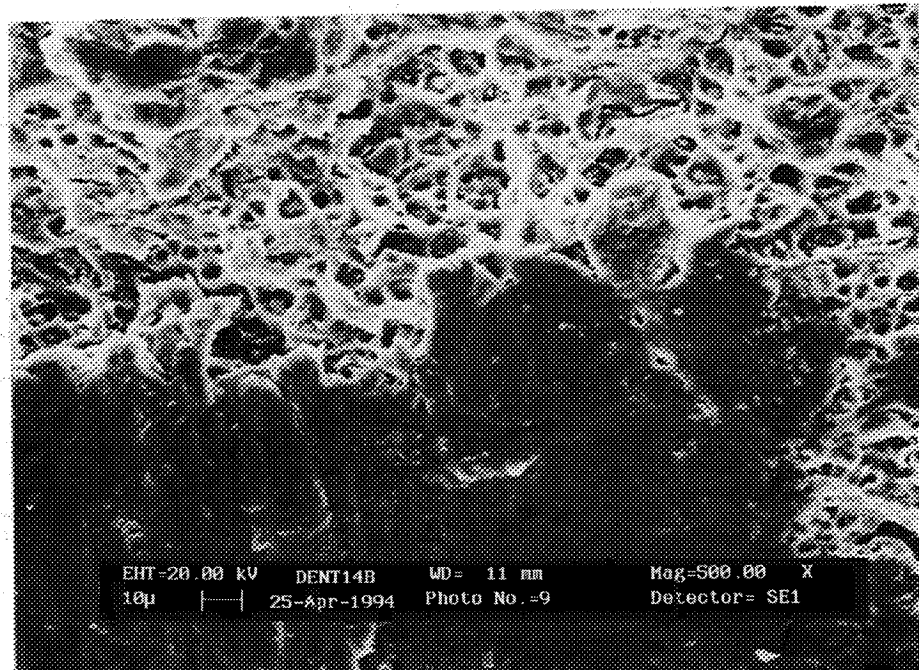
Figure 13. Scanning electron micrograph of the fracture surface in a region where crack contact has occurred. The region in the upper part of the picture shows no contact: the typical ductile fracture surface is seen. In the lower region the ductile fracture surface has been flattened and abraded by the crack surfaces sliding past each other.